PHYSICAL REVIEW B **95**, 081409(R) (2017)

# Bound states in nanoscale graphene quantum dots in a continuous graphene sheet

Jia-Bin Qiao,[1] Hua Jiang,[2] Haiwen Liu,[1] Hong Yang,[1] Ning Yang,[1] Kai-Yao Qiao,[1] and Lin He[1,*]

[1]*Center for Advanced Quantum Studies, Department of Physics, Beijing Normal University, Beijing 100875, People's Republic of China*

[2]*College of Physics, Optoelectronics and Energy, Soochow University, Suzhou 215006, People's Republic of China*

(Received 28 September 2016; revised manuscript received 6 December 2016; published 27 February 2017)

Considerable efforts have been made to trap massless Dirac fermions in a graphene monolayer, but only quasibound states have been realized in continuous graphene sheets up to now. Here, we demonstrate the realization of bound states in nanoscale graphene quantum dots (GQDs) in a continuous graphene sheet. The GQDs are electronically isolated from the surrounding continuous graphene sheet by circular boundaries, which are generated by strong coupling between graphene and the substrate. By using scanning tunneling microscopy (STM), we observe single-electron charging states of the GQDs, seen as Coulomb oscillations in the tunneling conductance. The evolution of single-electron tunneling of the GQDs between the Coulomb blockade regime and the Coulomb staircase regime is observed by tuning the STM tip-sample distances. Spatial maps of the local electronic densities reveal concentric rings inside the GQDs with each ring corresponding to a single Coulomb oscillation of the tunneling spectra. These results indicate explicitly that the electrons are completely trapped inside the nanoscale GQDs.

DOI: 10.1103/PhysRevB.95.081409

The confinement of electrons in a graphene monolayer faces challenges due to the Klein tunneling of massless Dirac fermions [1–3]. Although different recipes for confining the Dirac fermions in graphene have been suggested, only quasibound states with a finite trapping time have been realized very recently in a continuous graphene sheet with well-defined circular *p-n* junctions [4–6], even with some extremely external conditions [7–9], such as high magnetic fields, or supercritical charges. Here, we show that bound states can be formed in graphene quantum dots (GQDs), which are part of a continuous graphene sheet, with a circular boundary formed due to strong coupling with the substrate. In our scanning tunneling microscopy (STM) measurements, we used single-electron charging effects to identify the GQDs in the continuous graphene sheet. Single-electron charging phenomena are quite ubiquitous in atoms, molecules, and small isolated conducting islands. They are treated as a clear signature that the studied object is isolated from the surroundings by tunnel barriers, and the number of electrons residing on the object is quantized [10–16]. To observe single-electron charging phenomena, the resistance of each tunnel barrier isolating the studied object should be much larger than the quantum resistance ($R_q = h/e^2$), which ensures that the wave function of an excess electron on the studied object is well localized there. Previously, it was believed that single-electron charging states should not be observed in a continuous graphene sheet, and they have not been reported yet. Therefore, the observation of single-electron charging effects in the GQDs of the continuous graphene sheet, as reported in this Rapid Communication, provides direct evidence that Dirac fermions can be trapped in partial regions of the graphene monolayer.

In our experiment, a graphene monolayer was grown on molybdenum foils using the atmospheric pressure chemical vapor deposition method [17,18]. First, transition-metal carbide (TMC), such as $Mo_2C$, was formed from parent metal foils. Then, the thus-formed early $Mo_2C$ served as catalysts for graphene growth (details are described in the Supplemental Material [19]; see Figs. S1 and S2 for other characterizations of the sample, and Fig. S3 for the growth process). The STM investigation of the as-grown samples revealed the presence of a reconstructed $Mo_2C$ surface underneath the continuous graphene monolayer. These reconstructions of the TMC surface consist of nanoscale islands and quantum-dot-like vacancy islands [see Figs. 1(a) and S3 [19]]. The graphene monolayer is suspended over the vacancy islands of the surface, and the van der Waals forces from the STM tip can induce substantial mechanical deformation in the nanoscale suspended graphene membranes [20,21]. Our experiment indicates that the suspended graphene nanomembranes over the vacancy islands show a reversible mechanical deformation in response to the change of the tip-graphene distances, as shown in Fig. 1(b). There may be strong coupling between Mo atoms around the boundaries of the vacancy islands and the carbon atoms of graphene, which leads to the formation of boundaries with nanoscale widths [17,18,22,23]. Additionally, the charge transference between graphene and the TMC surface is expected to be affected by the spatial variation of distance between graphene and the TMC surface around the boundaries of the vacancy islands [24]. These two effects can result in electron confinement in partial regions of a continuous graphene sheet. We will show subsequently that the suspended graphene nanomembranes over the vacancy islands behave as isolated GQDs (from now on, we use GQDs to refer to the suspended graphene regions over the vacancy islands in this work).

Our scanning tunneling spectroscopy (STS) measurements, as shown in Fig. 1(c), indicate that the suspended graphene region exhibits quite different electronic properties compared to the surrounding graphene sheet. Inside the suspended graphene region we observe a series of almost equally spaced resonances in the tunneling conductance. Outside such a suspended graphene region we observe a V-shaped spectrum, as expected to be observed for a graphene monolayer on a metallic surface. Similar phenomena have also been observed

*helin@bnu.edu.cn

 

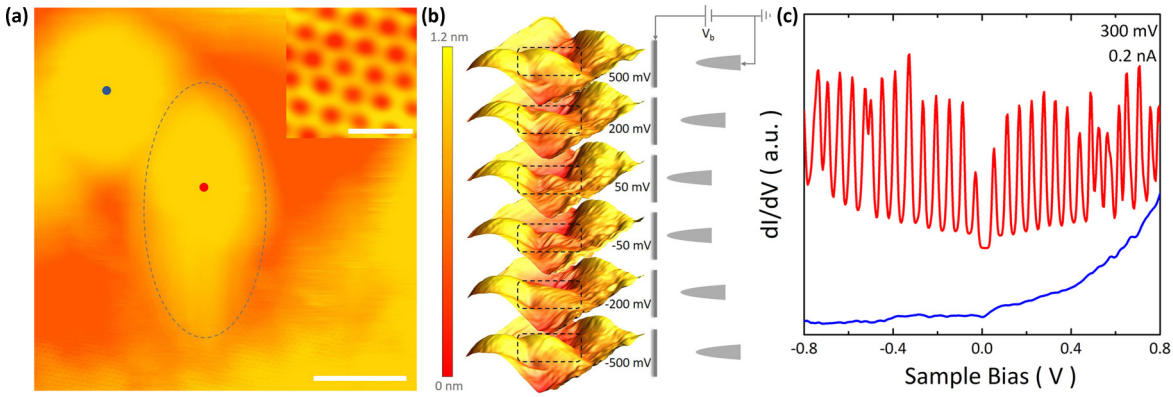


FIG. 1. STM and STS measurements around a GQD. (a) STM topographic image ($V_b = 500\,\text{mV}$, $I_S = 0.20\,\text{nA}$) showing a suspended graphene nanostructure over a vacancy island of the substrate, as marked with the ellipse-shaped dashed curve. The scale bar is 5 nm. The inset shows the atomic structure of graphene obtained in the studied region. The scale bar in the inset is 0.5 nm. The suspended graphene nanostructure behaves as an isolated GQD. (b) STM topographic images of the suspended graphene nanostructure over the vacancy island for different bias voltages (i.e., for different tip-sample distances). (c) Typical $dI/dV$ spectra recorded inside and outside of the suspended graphene nanostructure (the GQD). The curves are offset on the $Y$ axis for clarity. (a.u. = arbitrary units.)

around other suspended graphene regions in our experiment. The spatial variation of the tunneling spectra, as shown in Figs. 1(c) and S10 [19], precludes any possible artificial effects of the STM tips as the origin of these features. We attribute the peaks in the tunneling spectra recorded inside the suspended graphene regions to Coulomb oscillations, which are expected to be observed in the tunneling conductance of the isolated GQDs [10]. Such a result indicates that each suspended graphene region over the vacancy island is electronically isolated from the surrounding graphene sheet by an insulating barrier and behaves as a GQD. When the STM tip is positioned above a GQD, an asymmetric double-barrier tunnel junction (DBTJ), as schematically shown in Fig. 2(a), is formed. One of the tunnel barriers, described by a capacitor $C_T$ in parallel with an ohmic resistor $R_T$, is generated between the STM tip and the GQD; the other tunnel barrier, described by a capacitor $C_B$ in parallel with an ohmic resistor $R_B$, is generated between the GQD and the surrounding graphene sheet. Therefore, the tunneling spectra of the GQDs can be tuned by varying the tip-sample distances, and such a behavior should be described well by the orthodox Coulomb blockade theory [25,26].

To verify the above assumption, we measured the tunneling spectra of the GQD by varying the tip-sample distances, which can be realized by tuning the bias voltages or changing the tunneling currents during the STM measurement (see Fig. S5 [19]). The variation in the tip-sample distances changes the tunnel resistance $R_T$ dramatically and therefore affects the spectra of the GQD according to the effective circuit of the DBTJ. Figure 2(b) shows a representative result obtained in the GQD (see Fig. S5 for more experimental data [19]). For large tip-sample distances (large $R_T$), the spectra exhibit the typical signature of a Coulomb blockade (CB), i.e., a zero-conductance gap around the Fermi energy. For small tip-sample distances (small $R_T$), the spectra present quasiperiodic tunneling peaks, known as the signature of a Coulomb staircase (CS). Obviously, an evolution of the spectra between the CB regime and the CS regime is observed, as shown in Fig. 2(b), by a controlled change of the resistance $R_T$, i.e., the distance between the STM tip and the GQD. Such a result can be reproduced well by the optimized simulation based on the orthodox Coulomb blockade theory [25,26], as shown in Fig. 2(c). In the simulation, $R_B$ is assumed to be a constant and we only change the value of $R_T$ according to the experimental condition (some factors determining the shape and intensity of conductance peaks are taken into account; see the Supplemental Material for details [19]). The consistency between the experimental data and the theoretical results demonstrates explicitly that the suspended graphene region over the vacancy island behaves as an isolated GQD.

Here we should point out that the tunneling spectra of the nanoscale GQDs, as shown in Fig. 2(b), also exhibit two other important features beyond the description of the orthodox Coulomb blockade theory. The first one is the relatively wide distribution of the energy spacing between the nearest-neighbor tunneling peaks of the spectra. Figure 2(d) shows representative histograms of the nearest-neighbor level spacing of three GQDs observed in our experiment. The random tunneling peak spacing may arise from the roughness and irregular geometry of GQDs, which can be well described by the theory of chaotic neutrino billiards [10]. Moreover, the quantum confinement effect can also influence the tunneling peak spacing for nanoscale GQDs, and may alter the fitting parameters of the DBTJ model. However, the quantum confinement effect cannot change the qualitative features of Coulomb oscillation in the GQDs. Considering that the quantitative description of quantum confinement effect relays detailed information about the GQD boundaries, which is beyond the current experimental condition, we ignore the effect of quantum confinement in the theoretical simulations. The second feature beyond the description of the orthodox theory is the deviation between the histograms of the nearest-neighbor level spacing for electrons and holes, as shown in Fig. 2(d). There is a slight difference between the maxima of the histograms for electrons and holes. Figure 2(e) shows a representative result about the energy positions of the peaks as a function of the integer number obtained in a tunneling spectrum of a GQD (a similar result has been observed in

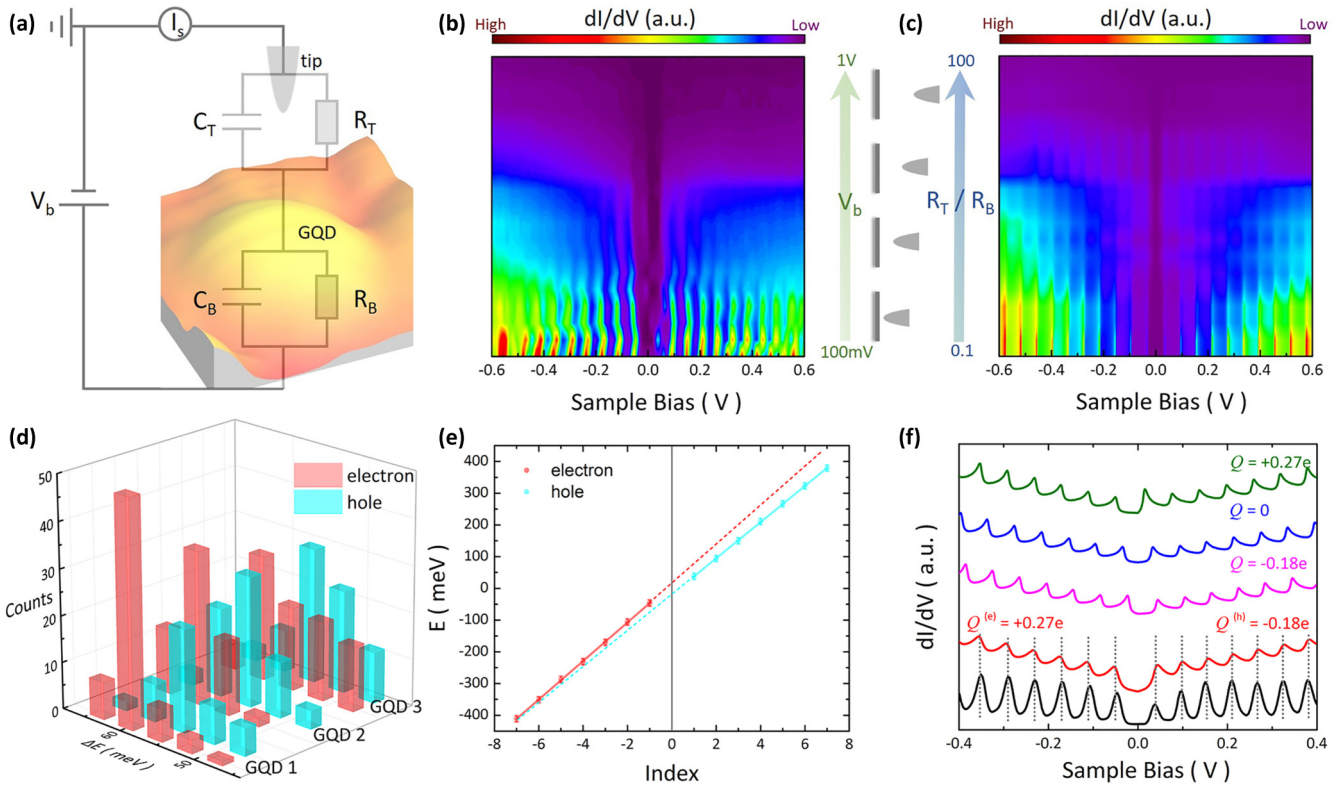


FIG. 2. Spectra of single-electron effects in the GQDs. (a) A DBTJ circuit where each junction is represented by a set of capacitors and resistors. The semitransparent background shows the schematic diagram of the single-electron charging system, in which the GQD is electronically isolated from the surrounding continuous graphene sheet. (b) shows representative STS spectra of a GQD by varying the bias voltages, i.e., the tip-sample distance. (c) shows simulated tunneling spectra of a GQD by changing the ratio of $R_T/R_B$. The parameters used in the calculation are $C_B = 2.67$ aF, $C_T = 0.1$ aF, $R_B = 1\,M\Omega$, and $Q = 0$. (d) Three-dimensional histogram of the nearest-neighbor level spacing of the conductance peaks in the STS spectra acquired on different GQDs. (e) Energy levels of conductance peaks, extracted from the spectra in the $dI/dV$ map shown in (b) at $V_b = 110$ mV, as a function of the peak index (electron, negative integer numbers; hole, positive integer numbers). The linear fitting of the data indicates a slight deviation of the average energy spacing of the nearest-neighbor peaks for electron and hole. (f) A typical STS spectrum of the GQD recorded at $V_b = 110$ mV (black line). The red curve is the simulated result by taking into account the electron-hole asymmetry. In the calculation, we used $C_B^{(e)} = 2.67$ aF, $C_B^{(h)} = 2.85$ aF, $Q^{(e)} = 0.27e$, and $Q^{(h)} = -0.18e$. The green, blue, and pink curves are also simulation results but without considering the electron-hole asymmetry. The remaining parameters in the calculation are $R_B = 1$ MΩ, $R_T = 0.2$ MΩ, and $C_T = 0.1$ aF.

all the spectra of the GQDs in our experiment). According to the slopes of the data, we can conclude that there is a notable difference between the average energy spacing of the nearest-neighbor tunneling peaks for electrons and holes. Such a behavior is attributed to electron-hole asymmetry in the graphene monolayer. The existence of electron-hole asymmetry in graphene has been previously demonstrated through Landau level spectroscopy [27,28,29] and transport measurements [30,31]. To better describe the experimental data using the orthodox theory, we assume different values of the capacitor $C_B$ for electrons and holes, i.e., we have $C_B^{(e)} \neq C_B^{(h)}$ (consequently, we have different residual charges for electrons and holes, i.e., $Q^{(e)} \neq Q^{(h)}$) to account for the electron-hole asymmetry in graphene. A moderate difference between the capacitor $C_B$ and the residual charges for electrons and holes well describes the observed electron-hole asymmetry in the tunneling spectra of the GQDs, as shown in Fig. 2(f).

The electronic properties of the GQDs are further studied by operating energy-fixed STS mapping. Figures 3(a) and 3(b) show two representative STS maps at different energies, which exhibit striking concentric rings of differential conductance peaks inside the GQDs. Each ring in the STS maps corresponds to a single Coulomb oscillation of the GQD [14,15]. When the STM tip is moved above the GQD, it induces spatial variation of band bending in the GQD [32,33], as schematically shown in Fig. 3(c). This tip-induced gating leads to maxima in the measured STS maps at certain positions, where the Fermi levels cross one of the tunneling peaks in the spectra. The gate-dependent band-bending mechanism explains the nearly concentric rings seen in each GQD in the conductance maps. Such a result further demonstrates that the suspended graphene regions over the vacancy islands (the GQDs) are electronically isolated from the surrounding graphene sheet.

It is now natural to ask how the electrons are confined in the GQDs in the continuous graphene sheet. The spatial variation of distance between graphene and the TMC surface around the boundaries of the vacancy islands can generate a nanoscale circular $p$-$n$ junction [24] in the graphene sheet (see Fig. S8 [19]). To explore the effect of nanoscale circular

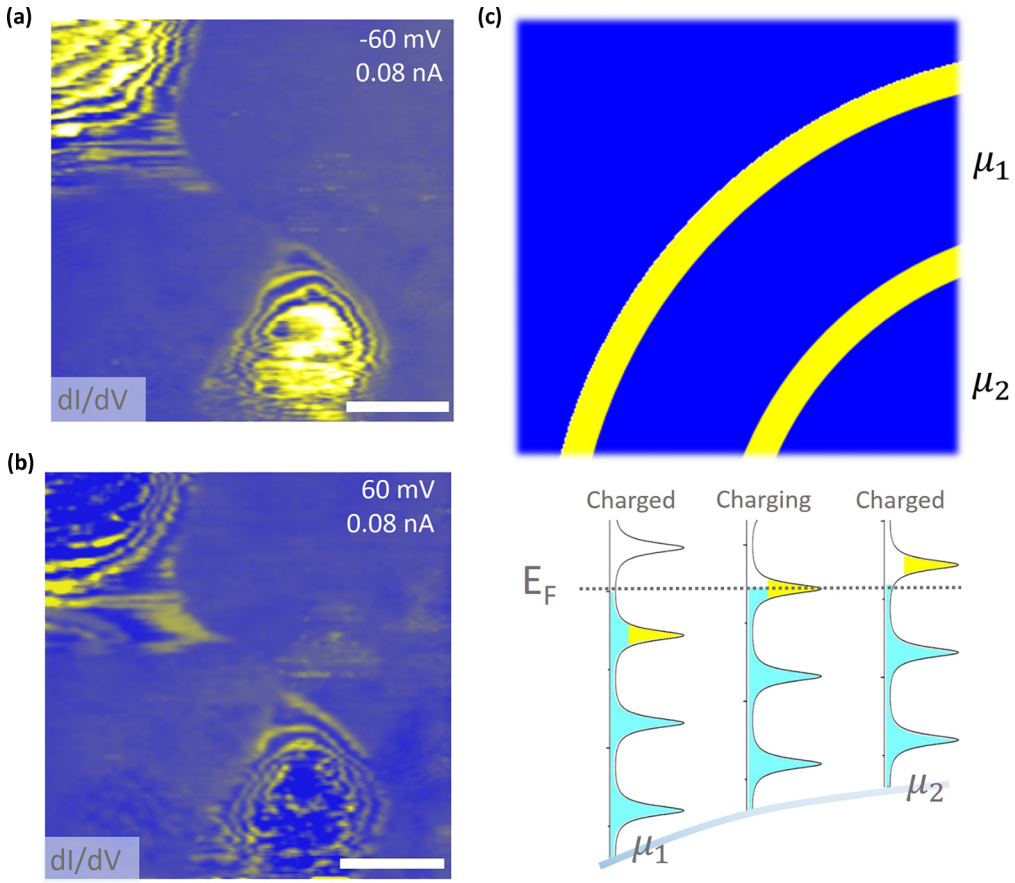


FIG. 3. Imaging the single-electron states in the GQDs. (a), (b) $dI/dV$ maps recorded around the GQDs with a fixed sample bias of (a) −60 and (b) 60 mV, respectively. The scale bar is 5 nm. There are two sets of concentric rings of conductance peaks, centered at two different GQDs. Each ring in the STS maps corresponds to a single Coulomb oscillation on the GQD. (c) A schematic diagram showing effects of tip-induced band bending on the formation of the concentric rings inside the GQDs in the conductance maps.

*p-n* junctions on the electronic properties of the GQDs in the graphene sheet, we studied a similar structure, i.e., a GQD in a continuous graphene sheet, grown on a Cu foil for comparison. The electrons are temporarily trapped inside the circular *p-n* junction to form the quasibound states [4–6], as revealed by a series of resonance peaks at negative energies in the tunneling spectra (see Fig. S14 in the Supplemental Material for experimental data and Fig. S15 for our simulation results [19]). Both experiment and theory demonstrate that the lowest resonance of the quasibound states exhibits maxima near the center of the GQD, whereas higher resonances display a stronger intensity close to the boundary of the GQD (see Figs. S14 and S15 [19]), as reported previously in Ref. [6]. Obviously, the main features of the single-electron transport in the GQD on the TMC surface, as shown in Figs. 2 and 3, are different from those of the quasibound states inside the circular *p-n* junction on the Cu surface, as shown in Fig. S14 [19]. We attributed the origin of the difference to the different graphene-substrate coupling: Graphene is strongly chemisorbed on TMC, whereas the binding to Cu is much weaker. The existence of nanoscale boundaries where the carbon atoms of graphene are strongly coupled with Mo atoms around the boundaries of the vacancy islands may play a critical role in the electron confinement in the GQDs.

To further explore the origin of the tunnel barrier between the GQDs and the surrounding continuous graphene sheet, we measured atomic-resolved STS spectra around the boundary of the GQD by fixing the tip-sample distance (the resistance $R_T$), as shown in Figs. 4(a) and 4(b). When approaching the boundary from the inside of the GQD, we observed the evolution of the spectra from the CS regime to the CB regime. This indicates that the $R_B$ decreases dramatically from position (i) to position (iii) [see Fig. 4(c)]. The most striking result is that the spectrum recorded at position (iv) becomes V shaped, as expected to be observed in the continuous graphene sheet. Such a result indicates that the effective boundary of the GQD spreads over position (i) to position (iii), with a typical width of several nanometers. In graphene, the $\pi$ electrons are responsible for the electronic properties at low energies. Owing to the strong graphene-Mo interaction, the $\pi$ orbital of the graphene is hybridized with the $d$ orbital of the Mo atoms within the boundary regions, and these $\pi$ electrons around the boundary become strongly localized (see the illustration in Fig. S3 [19]). Therefore, the electrons inside the GQD are strongly confined. The confinement of electrons due to the tunnel barrier between GQD and the continuous graphene sheet is further demonstrated through imaging the intervalley scattering around the boundary of the GQD, as shown in Fig. 4(d). The existence of valley mixing is seen as

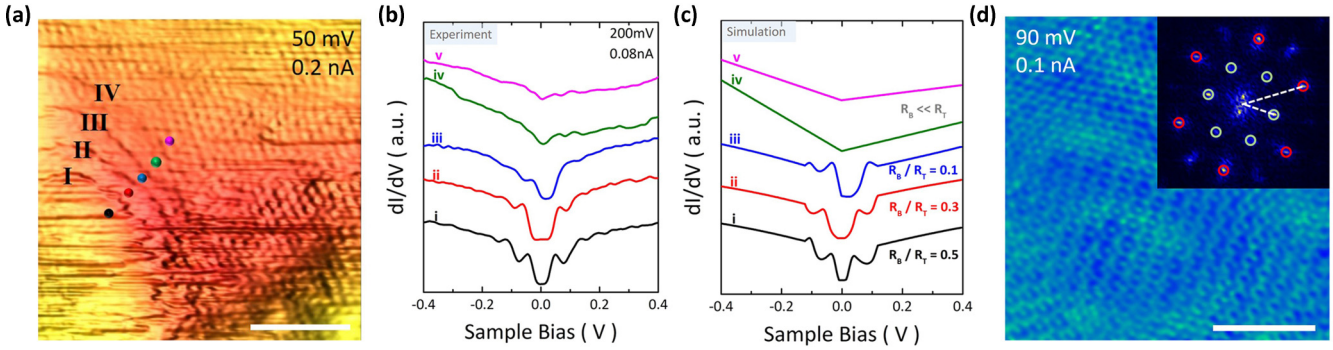


FIG. 4. STS spectra and valley mixing around the atomically sharp boundary of the GQD. (a) Zoom-in atomic-resolution topographic images obtained at the top right corner of the GQD. The scale bar is 2 nm. (b) STS spectra recorded at different positions in (a) (indicated by colored dots) by fixing the tip-sample distance. (c) Simulated tunneling spectra of a GQD by changing the ratio of $R_B/R_T$. In the simulation, $R_T$ is fixed according to the experiment. The dramatic changes of the spectra recorded at positions (i) and (iv) indicate that the effective width of the boundary of the GQD is about 2 nm. (d) A representative STS map recorded around the boundary of the GQD. A clear interference pattern arising from the intervalley scattering is observed. The inset shows the fast Fourier transform of the STS map. The six outer spots are the reciprocal lattice of graphene and the six inner spots arise from valley mixing induced by the boundary of the GQD.

the emergence of both the $\sqrt{3} \times \sqrt{3}R30^\circ$ interference pattern of carbocyclic rings in the STS maps and the six inner spots in the fast Fourier transform image [34,35]. Although further analysis is necessary, our results indicate that the atomically sharp boundaries induced by a strong graphene-substrate interaction are very important in the electron confinement in the GQDs.

In summary, bound states are realized in nanoscale GQDs in a continuous graphene sheet. Our result indicates that strong graphene-substrate coupling plays a vital role in confining electrons in the nanoscale GQDs. The method reported in here may pave the way to electronically isolate graphene nanostructures in a continuous graphene monolayer, which is very important in advanced graphene nanoelectronics.

This work was supported by the National Basic Research Program of China (Grants No. 2014CB920903, No. 2013CBA01603, and No. 2014CB920901), the National Natural Science Foundation of China (Grants No. 11674029, No. 11422430, No. 11374035, No. 11374219, and No. 11504008), and the program for New Century Excellent Talents in University of the Ministry of Education of China (Grant No. NCET-13-0054). L.H. also acknowledges support from the National Program for Support of Top-notch Young Professionals.

[1] M. I. Katsnelson, K. S. Novoselov, and A. K. Geim, Chiral tunneling and the Klein paradox in graphene, Nat. Phys. **2**, 620 (2006).

[2] A. F. Young and P. Kim, Quantum interference and Klein tunneling in graphene heterojunctions, Nat. Phys. **5**, 222 (2009).

[3] W.-Y. He, Z.-D. Chu, and L. He, Chiral Tunneling in a Twisted Graphene Bilayer, Phys. Rev. Lett. **111**, 066803 (2013).

[4] Y. Zhao, J. Wyrick, F. D. Natterer, J. Rodriguez-Nieva, C. Lewandowski, K. Watanabe, T. Taniguchi, L. Levitov, N. B. Zhitenev, and J. A. Stroscio, Creating and probing electron whispering gallery modes in graphene, Science **348**, 672 (2015).

[5] J. Lee *et al.*, Imaging electrostatically confined Dirac fermions in graphene quantum dots, Nat. Phys. **12**, 1032 (2016).

[6] C. Gutiérrez, L. Brown, C.-J. Kim, J. Park, and A. N. Pasupathy, Klein tunneling and electron trapping in nanometre-scale graphene quantum dots, Nat. Phys. **12**, 1069 (2016).

[7] S. Jung *et al.*, Evolution of microscopic localization in graphene in a magnetic field from scattering resonances to quantum dots, Nat. Phys. **7**, 245 (2011).

[8] Y. Wang, D. Wong, A. V. Shytov, V. W. Brar, S. Choi, Q. Wu, H.-Z. Tsai, W. Regan, A. Zettl, R. K. Kawakami, S. G. Louie, L. S. Levitov, and M. F. Crommie, Observing atomic collapse resonances in artificial nuclei on graphene, Science **340**, 734 (2013).

[9] J. Mao, Y. Jiang, D. Moldovan, G. Li, K. Watanabe, T. Taniguchi, M. R. Masir, F. M. Peeters, and E. Y. Andrei, Realization of a tunable artificial atom at a supercritically charged vacancy in graphene, Nat. Phys. **12**, 545 (2016).

[10] L. Ponomarenko *et al.*, Chaotic Dirac billiard in graphene quantum dots, Science **320**, 356 (2008).

[11] K. A. Ritter and J. W. Lyding, The influence of edge structure on the electronic properties of graphene quantum dots and nanoribbons, Nat. Mater. **8**, 235 (2009).

[12] A. Deshpande, W. Bao, Z. Zhao, C. N. Lau, and B. LeRoy, Imaging charge density fluctuations in graphene using Coulomb blockade spectroscopy, Phys. Rev. B **83**, 155409 (2011).

[13] P. Fallahi *et al.*, Imaging a single-electron quantum dot, Nano Lett. **5**, 223 (2005).

[14] A. C. Bleszynski *et al.*, Scanned probe imaging of quantum dots inside InAs nanowires, Nano Lett. **7**, 2559 (2007).

[15] M. T. Woodside and P. L. McEuen, Scanned probe imaging of single-electron charge states in nanotube quantum dots, Science **296**, 1098 (2002).

[16] X. Wang, Y. Ouyang, L. Jiao, H. Wang, L. Xie, J. Wu, J. Guo, and H. Dai, Graphene nanoribbons with smooth edges behave as quantum wires, Nat. Nanotechnol. **6**, 563 (2011).

[17] B. Dai *et al.*, Rational design of a binary metal alloy for chemical vapour deposition growth of uniform single-layer graphene, Nat. Commun. **2**, 522 (2011).

[18] Z. Zou, L. Fu, X. Song, Y. Zhang, and Z. Liu, Carbide-forming groups IVB-VIB metals: A new territory in the periodic table for CVD growth of graphene. Nano Lett. **14**, 3832 (2014).

[19] See Supplemental Material at http://link.aps.org/supplemental/10.1103/PhysRevB.95.081409 for methods, more STM images, STS spectra, and details of the analysis.

[20] N. N. Klimov *et al.*, Electromechanical properties of graphene drumheads, Science **336**, 1557 (2012).

[21] T. Mashoff *et al.*, Bistability and oscillatory motion of natural nanomembranes appearing within monolayer graphene on silicon dioxide, Nano Lett. **10**, 461 (2010).

[22] H. Lim, J. Jung, R. S. Ruoff, and Y Kim, Structurally driven one-dimensional electron confinement in sub-5-nm graphene nanowrinkles, Nat. Commun. **6**, 8601 (2015).

[23] S.-Y. Li, M. Zhou, J.-B. Qiao, W. Duan, and L. He, Wide-band-gap wrinkled nanoribbon-like structures in a continuous metallic graphene sheet, Phys. Rev. B **94**, 085419 (2016).

[24] P. A. Khomyakov, G. Giovannetti, P. C. Rusu, G. Brocks, J. van den Brink, and P. J. Kelly, First-principles study of the interaction and charge transfer between graphene and metals, Phys. Rev. B **79**, 195425 (2009).

[25] A. Hanna and M. Tinkham, Variation of the Coulomb staircase in a two-junction system by fractional electron charge, Phys. Rev. B **44**, 5919 (1991).

[26] M. Amman, R. Wilkins, E. Ben-Jacob, P. Maker, and R. Jaklevic, Analytic solution for the current-voltage characteristic of two mesoscopic tunnel junctions coupled in series, Phys. Rev. B **43**, 1146 (1991).

[27] K.-K. Bai *et al.*, Detecting giant electron-hole asymmetry in a graphene monolayer generated by strain and charged-defect scattering via Landau level spectroscopy, Phys. Rev. B **92**, 121405(R) (2015).

[28] G. Li, A. Luican, and E. Y. Andrei, Scanning Tunneling Spectroscopy of Graphene on Graphite, Phys. Rev. Lett. **102**, 176804 (2009).

[29] S.-Y. Li *et al.*, Observation of unconventional splitting of Landau levels in strained graphene, Phys. Rev. B **92**, 245302 (2015).

[30] R. S. Deacon, K.-C. Chuang, R. J. Nicholas, K. S. Novoselov, and A. K. Geim, Cyclotron resonance study of the electron and hole velocity in graphene monolayers, Phys. Rev. B **76**, 081406(R) (2007).

[31] A. Kretinin, G. L. Yu, R. Jalil, Y. Cao, F. Withers, A. Mishchenko, M. I. Katsnelson, K. S. Novoselov, A. K. Geim, and F Guinea, Quantum capacitance measurements of electron-hole asymmetry and next-nearest-neighbor hopping in graphene, Phys. Rev. B **88**, 165427 (2013).

[32] V. W. Brar *et al.*, Gate-controlled ionization and screening of cobalt adatoms on a graphene surface, Nat. Phys. **7**, 43 (2011).

[33] D. Wong *et al.*, Characterization and manipulation of individual defects in insulating hexagonal boron nitride using scanning tunneling microscopy, Nat. Nanotechnol. **10**, 949 (2015).

[34] G. M. Rutter *et al.*, Scattering and interference in epitaxial graphene, Science **317**, 219 (2007).

[35] P. Mallet, I. Brihuega, S. Bose, M. M. Ugeda, J. M. Gomez-Rodriguez, K. Kern, and J. Y. Veuillen, Role of pseudospin in quasiparticle interferences in epitaxial graphene probed by high-resolution scanning tunneling microscopy, Phys. Rev. B **86**, 045444 (2012).